Nanoscale

Accepted Manuscript

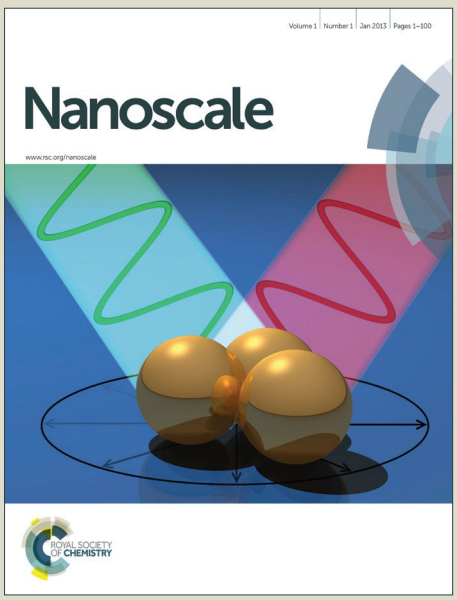

ROYAL SOCIETY OF CHEMISTRY

www.rsc.org/nanoscale

Journal Name

ARTICLE

Layering of Ionic liquids on Rough Surfaces

Received 00th January 20xx,
Accepted 00th January 20xx

DOI: 10.1039/x0xx00000x

www.rsc.org/

Alexis Sheehan[a], L. Andres Jurado[a], Shivaprakash N. Ramakrishna[b], Andrea Arcifa[b], Antonella Rossi[b,c], Nicholas D. Spencer[b], and Rosa M. Espinosa-Marzal[a]

Understanding the behavior of ionic liquids (ILs) either confined between rough surfaces or in rough nanoscale pores is of great relevance to extend studies performed on ideally flat surfaces to real applications. In this work we have performed an extensive investigation of the structural forces between two surfaces with well-defined roughness (<9 nm RMS) in 1-hexyl-3-methylimidazolium bis(trifluoromethylsulfonyl)imide by atomic force microscopy. Statistical studies of the measured layer thicknesses, layering force, and layering frequency reveal the ordered structure of the rough IL-solid interface. Our work shows that the equilibrium structure of the interfacial IL strongly depends on the topography of the contact.

Introduction

Room Temperature Ionic Liquids are organic salts with melting points below 100°C. Although first discovered in the mid-1900s, they have recently become the topic of intensive scientific research, in particular for applications such as electrolytes for electrochemical cells and as lubricants. [1-3] Ionic liquids are typically composed of large, asymmetric organic molecules that are non-uniformly charged.[4] This molecular structure leads to higher charge densities and electrochemical stabilities than most conventional electrolytes used in electrochemical cells. [4-6] The vapor pressures of ILs are extremely low over a wide temperature range, which is advantageous for high-temperature applications and a prerequisite for applications in vacuum.[7] Moreover, physical and chemical properties can be tuned by individually changing the molecular composition of anion and cation.

The investigated ILs form a layered structure–denoted as solid-like—at the solid-liquid interface. The layering is a result of ion-substrate and ion-ion interactions (van der Waals, hydrogen bonding, π-π interactions, solvophobic, and Coulombic), ion shape, size, and packing (see e.g. refs.[8-16]). IL layering is further enhanced under nanoconfinement as a result of the proximity of both IL-solid interfaces.[12, 17] Understanding the structures of nanoconfined ILs is important for their use as electrolytes, since it determines the electrical double layer,[30-32] and as lubricants because it can determine the friction mechanism.[18, 19] Structural information of the solid-IL interface has been obtained by X-ray reflectivity,[16] neutron reflectometry,[20] sum-frequency vibrational spectroscopy,[21] X-ray photoelectron spectroscopy (XPS),[22-26] atomic force microscopy (AFM) imaging,[9, 10, 27-33] and the surface forces apparatus (SFA).[8, 11-15, 34-40] AFM and SFA force isotherms reveal film-thickness transitions as either a single layer of ions, or ion pairs, are collectively squeezed out from the confined region. The out-of-plane order is most pronounced at the solid-IL interface, decaying with distance from the substrate surface, and typically vanishing beyond ~3-7 layers. AFM imaging has revealed in-plane ordering of the ions at the IL-solid interface.[41]

[a] University of Illinois at Urbana-Champaign, Urbana 61801, Illinois, USA.
[b] ETH Zurich, 8093 Zurich, Switzerland.
[c] Università degli Studi di Cagliari, 09042, Italy.

† Footnotes relating to the title and/or authors should appear here.
Electronic Supplementary Information (ESI) available: optimized geometries and sizes for [HMIM] Ntf2, SEM images of the smooth and rough colloids, frequency of occurrence of layering in the resolved force-distance curves for all investigated systems with [HMIM] Ntf2, layer size and layering force measured with a sharp tip on mica for the same IL, and results of the kinetics experiments.
See DOI: 10.1039/x0xx00000x

Several parameters have been found to influence the structure and dynamics of nanoconfined IL layers, such as the chemical composition of the surface,[42] surface charge and potential,[17, 27, 43, 44] the presence of an external electrical field,[45] and the strength of interactions among the ions.[46] It has been shown that small amounts of water absorbed from ambient air are able to modify the layered structure of the confined IL.[47,48-50] One parameter that has not yet been examined is the effect of *roughness* on the interfacial structure of ILs.

Typical carbonaceous electrodes have *rough*, porous surfaces with roughness values ranging from the atomic up to the micrometer scale; similarly, roughness is significant on sliding steel surfaces and other materials. In contrast, most studies of the interfacial behavior of ILs have focused on atomically flat surfaces. Understanding IL behavior at rough surfaces could contribute toward the understanding of IL behavior in real systems and thus, ultimately, to improving their performance.

Force measurements show the layering of molecules confined between two surfaces as an oscillatory force with a superposed, monotonically attractive or repulsive component, which is known as a structural or solvation force. It is generally accepted that the oscillatory force is smeared out on rough surfaces, if the roughness is larger than the molecular dimension.[51] Simulations show that a significant dampening of the oscillatory force occurs on fluids confined between rough pores.[52] Recent experimental and modelling efforts have studied the effects of graphite surface defects on IL layering; AFM force measurements reveal less pronounced ordering on step-edge defects, as compared to flat regions[53], and molecular-dynamics studies found correlations between the ion size and the thickness of the graphite step-edge defect on the interfacial structure of the IL[54]. No systematic studies of the roughness effect on IL-layering have been reported to date.

In this work, we evaluate the interfacial structure of 1-hexyl-3-methylimidazolium bis(trifluoromethylsulfonyl)imide, on SiO_2 substrates as a function of nanometer-scale roughness (0.4-3.8 nm RMS). The counter-surface roughness is also varied (1 - 9 nm RMS) to investigate the equilibrium structure of a nanoconfined IL within a rough pore with a maximum width given by the asperity height (~26 nm). Force isotherms demonstrate the presence of multiple IL-layers with different characteristics that are evaluated in this work.

Materials and Methods

1-hexyl-3-methylimidazolium bis(trifluoromethylsulfonyl)imide ([HMIM] Ntf2) (purity 99%, Iolitec , Alabama, USA) was selected for this study. Figure SM1 (Supplementary information) shows the size of each ion, as determined by molecular mechanics with the Avogadro software (Version 1.0.3). [HMIM] Ntf2 was equilibrated at 44% RH and 20-25 °C for 3.5 days. Water uptake of [HMIM] Ntf2 equilibrated at 44%RH was found to be ~0.2% in weight, as determined by thermogravimetric analysis. Force measurements were performed under ambient laboratory conditions (44-50% RH), i.e. a slight uptake of water during the experiments cannot be ruled out.

Preparation of rough substrates

Silicon wafers (p-type Boron <111> 500 µm, WRS, USA) were cut to 1 cm x 3 cm using a diamond pen. The cut silicon substrates were cleaned by ultrasonication in toluene, isopropanol and ethanol (solvent from Sigma Aldrich, St. Louis, USA) in succession, three times in each solvent for 15 minutes.

The rough substrates were prepared following the protocol in refs.[55-57] Briefly, a 50% solution of branched polyethyleneimine (PEI) with a molecular weight of 750 kDa (Sigma Aldrich, St. Louis, USA) was diluted to a concentration of 0.5 mg/mL in deionized water and stirred overnight at 50 °C to ensure dissolution of the polymer. The PEI solution was filtered twice before use, with a 0.2 µm syringe filter. The wafers were UV-ozone treated for 30 minutes, then immersed for 30 minutes in the prepared PEI solution to allow adsorption of the polymer onto the wafer. Following adsorption of the polymer, the substrates were rinsed thoroughly with Milli-Q water. A suspension of silica nanoparticles (NPs) (5% concentration, 12 nm nominal diameter, Microspheres-Nanospheres, NY, USA) was diluted in deionized water to a concentration of 0.002 weight % and ultrasonicated for 15 minutes directly before use. The PEI-coated wafer was then approached vertically to the NP suspension (~45 ml), until one of the 1 cm-edges was immersed into the solution (~1 mm) and held for five minutes to eliminate capillary effects in the rest of the wafer. Then, the entire wafer was completely submerged in the suspension and held for a set time between 5 and 30 minutes to achieve different number densities of surface-adsorbed NPs (given as number of NPs per μm^2). After immersion, the small beaker containing the NP suspension and the wafer were placed in a larger beaker (~300 ml), and the larger beaker was filled completely with Milli-Q water to dilute the NP suspension. The wafer was removed slowly from the solution.

Bare silicon wafers (as reference flat surfaces) and the nanoparticle-coated surfaces were sintered up to 1080 °C using a heating ramp of 10 °C/min, followed by a cooling ramp of 2 °C/min. Sintering leads to a naturally oxidized top layer of SiO_2 on the silicon wafers;[58] we will refer to them as *silica substrates* in the following. The substrates were cleaned according to the previously described solvent cleaning method, and then UV-ozone treated for 30 minutes immediately before force measurements. After force measurements were performed, the substrates were immersed in acetone overnight and then cleaned according to the above-described method before further use.

Atomic Force Microscopy (AFM) Imaging

AFM images of rough and flat silica substrates were collected in AC mode at scan rates of 1Hz in air with an MFP-3D (Asylum Research, California, USA) using gold-coated silicon cantilevers with a sharp tip of nominal radius of less than 10 nm, a resonant frequency of approximately 300 kHz, and nominal spring constant of 20-75 N/m (Budget Sensors, Bulgaria). Tips were UV-ozone treated for at least 30 minutes prior to use.

The image scan sizes were 500nm x 500nm, 1µm x 1µm and 5µm x 5µm. The roughness of the silica substrates was characterized by the number of NPs per μm^2, which were counted manually on six images for each substrate. To determine the average distance between NPs, nine lines were considered on each image, and the average distance was determined from the scan-line size divided by the number of NPs. Peak-to-valley and asperity-to-asperity distances were obtained by averaging at least 10 profiles per image at three separate locations for each of the substrates used. Various "flat" sintered substrates (i.e. with a NP surface density of 0 μm^{-2}) were used in force measurements, while only two rough substrates were employed through all experiments –one that was immersed for 10 minutes in the NP suspension and another one that was immersed for 30 minutes– to investigate two statistically different characteristic roughness values.

The roughness of the silica colloids glued to tipless cantilevers (used for AFM force measurements) was determined through AFM reverse imaging at the approximate contact area. A TGTZ-400 test grating (Ted Pella, Redding, CA, USA) was used to reverse-image the colloids. 10 µm nominal diameter SiO_2 colloids (Microspheres-Nanospheres, New York, USA) were glued with NOA 63 optical glue (Norland, New Jersey, USA) to tipless silica cantilevers (Mikromasch, Tallinn, Estonia) with nominal spring constants of approximately 0.2 N/m. Immediately prior to imaging, the cantilevers with glued colloids were rinsed with ethanol, followed by 40 minutes of UV-ozone treatment. Images were collected in contact mode at scan rates between 0.8 – 1.0 Hz in air with a JPK Nanowizard Ultra (JPK Instruments, Berlin, Germany). At least 10 cross-sections per image were analyzed to determine average height, asperity-to-asperity distance and the RMS roughness, on at least three different colloids per batch.

Force Measurements by AFM

Force measurements were obtained using an MFP-3D (Asylum Research, California, USA) in contact mode using both sharp silicon tips (CSC38/No Al, radius <10 nm, normal spring constant k of 0.3-0.9 N/m, Mikromasch, Estonia), and tipless silicon cantilevers (CSC37/tipless/Al Bs, k=0.03-0.09 N/m, Mikromasch, Estonia) glued to 10 µm diameter SiO_2 colloids (Microspheres-Nanospheres, New York, USA). The spring constant of all AFM tips was determined by the thermal-noise method.[59] All tips were UV-ozone treated for 30 minutes immediately prior to use.

A droplet of ~125 µL of [HMIM] Ntf2 was pipetted onto the substrate. After an equilibration time of at least 2 h, normal force vs. distance isotherms were determined on 5 µm x 5 µm force maps with a total of 576 force measurements for each substrate-tip combination. The approach speed was maintained constant at 30 nm/s and the maximum applied force was 8 nN. X-Y piezo velocity was 50 nm/s during force mapping to reduce noise.

According to ref. [49] it takes 6 hours to achieve the equilibrium interfacial structure on a mica surface, which the authors relate to the slow dissolution of interfacial potassium and surface hydration; in contrast, the formation of the equilibrium interfacial layer was found to be spontaneous on gold, and therefore it appears to be strongly influenced by the substrate-IL interactions. In force maps, we probe the structure at different locations on the substrate, but at the same position on the tip/colloid; thus, the IL structure on the tip/colloid is disturbed during a force measurement. To be sure that we probe the equilibrium IL-structure in force maps, we have investigated the kinetics of interfacial structure formation in separate experiments (called kinetic experiments) by varying the time delay (from 10 s to 7 min) between consecutive force measurements to allow the re-formation of the IL-structure on the tip/colloid.

After the force measurements, the tips were immersed in acetone overnight, then in isopropanol overnight and finally in ethanol for at least 2 hours. The tips were dried and treated with UV-ozone for 30 minutes before further use.

Scanning Electron Microscopy (SEM)

SEM images of the silica colloids were collected with an S4700 SEM (Hitachi, Tokyo, Japan). Images were collected under a variety of accelerating voltages and probe currents in an attempt to increase resolution and contrast. Ultimately, relatively low accelerating voltages (1 – 2 kV) were used since the penetration depth of the incident electrons is reduced, thus more directly probing the surface features.

Experimental Results

Roughness Characterization

The density of surface-adsorbed NPs is dependent on the immersion time in the NP suspension.[55, 56] The selected immersion times of the substrates for force measurements are 0 min (flat substrate), 10 min, and 30 min, with corresponding NP surface densities of 0, 170± 7 μm^{-2} , and 1100± 65 μm^{-2}, respectively. The average distance between the NPs is ~108±24 nm and ~51±6 nm for average surface densities of 170 μm^{-2} and 1100 μm^{-2}, respectively. AFM images of substrates with different NP densities are shown in Figure 1. The cross-sections are shown below each image, and the characteristics of the topography calculated by Gwyddion software (Version 2.41) are given in the table. The RMS roughness is ~1.80 nm for the 170 μm^{-2} and ~3. 8 nm for the 1100 μm^{-2} substrate.

The selected colloids (R=5µm) were from two different batches that had very different roughness values (see Figure 2a-b and SEM images in Figure SM2 in the Supplementary Information). The SEM images demonstrate that it is important to determine the roughness in the contact region, since it is not uniform over the entire sphere. The RMS roughness was statistically different for the two batches: 1.4±1.1 nm vs. 9.0±3.4 nm; the standard deviation shows the high variability of the topography. We will henceforth denote the two colloids as "smooth" and "rough", respectively. Although the average asperity distance for both SiO_2 colloids is larger than that for the rough substrates, it is important to note that the peak-to-

valley distance is larger for the rough colloid (20.7 nm) than for the substrates.

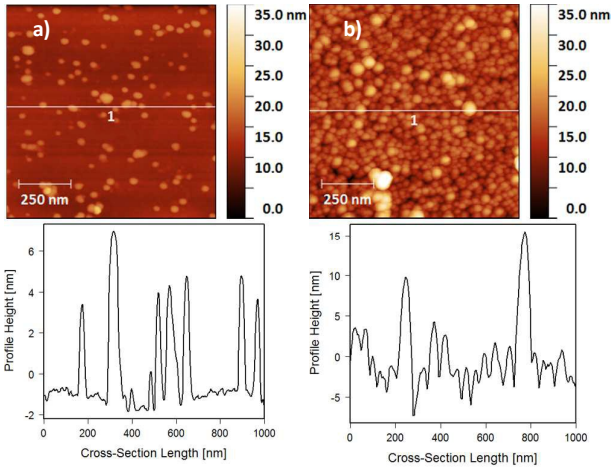

c)	Average RMS roughness [nm]	Average Peak-to-Valley distance [nm]	Average Asperity Distance [nm]
0 μm^{-2}	0.4		
170 μm^{-2}	1.8 (0.6)	4.8 (1.6)	107.5 (24.4)
1100 μm^{-2}	3.8 (1.4)	6.4 (1.1)	50.8 (5.6)

Figure 1: AFM images and corresponding cross-sections (1 µm x 1 µm) of silica substrates with surface densities of a) 170 μm^{-2} and b) 1100 μm^{-2}. AFM images were taken in air, in AC mode. The NPs appear larger (and therefore closer) than they are because the tip cannot perfectly follow the NP profile up to the surface.

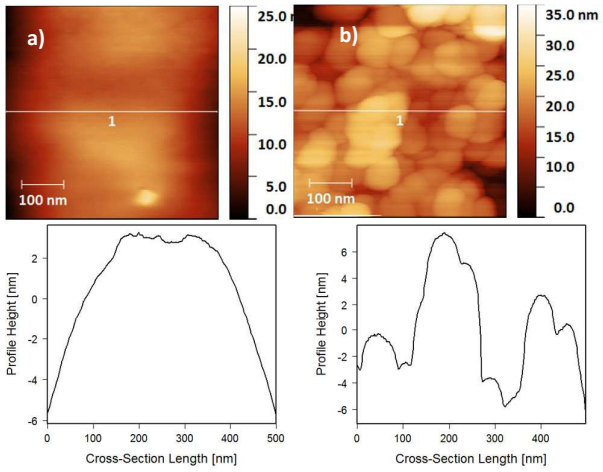

c)	Average RMS roughness [nm]	Average Peak-to-Valley distance [nm]	Average Asperity Distance [nm]
Batch 1 (rough)	9.0 (3.4)	20.7 (7.1)	204.9 (61.1)
Batch 2 (smooth)	1.4 (1.1)	2.5 (1.9)	123.4 (37.3)

Figure 2: Representative AFM images (500 nm x 500 nm) and cross-sections in a region containing the contact area with the substrate of **a)** smooth and **b)** rough 10µm SiO_2 beads; **c)** The table gives the roughness characteristics (average RMS roughness, peak-to-valley distance and average lateral distance between asperities) obtained on at least 10 profiles per image over three images.

Force-Distance Isotherms

Representative force-distance isotherms for [HMIM] Ntf2 either confined between a SiO_2 colloid and a silica substrate, or measured with a sharp tip on the silica substrate, are shown in Figures 3, 4 and 5. To characterize the heterogeneity of the rough substrates (with NPs), force isotherms were obtained in force maps (5µmx5µm). All force isotherms exhibit a short-range repulsion, similar to previously reported AFM measurements for other ILs.[32] Due to the uncertainty of the absolute tip-substrate separation in AFM force measurements, we note that the abscissa has an *arbitrary zero* but we refer to it as "separation" in the following.

The statistical analysis discussed here was carried out on ~300 force-distance curves measured with a sharp tip, ~150 force-distance curves measured with a smooth colloid, and ~150 with a rough colloid. Interfacial IL layering was resolved in ~60-70% of the measured force isotherms in force maps with either a sharp tip, smooth colloid, or rough colloid. Figures 3-5 demonstrate the layering of [HMIM] Ntf2 on both flat and rough substrates probed with a sharp tip, and with SiO_2 colloids with RMS roughnesses ranging from 1 to 9 nm.

Force measurements with a sharp tip. Representative force-distance curves obtained with a sharp tip for the IL equilibrated with ambient air for the three substrates are shown in Figure 3; different colors were used to distinguish between force-distance curves on the same substrate measured during a force map, i.e. at different positions. We note that the Derjaguin approximation is only valid for radii R>> D, the surface separation; as the tip radius is of the same order of magnitude as the onset of repulsion, the Derjaguin approximation cannot be applied to this set of experiments and the force is reported in nN in this paper.

The measured normal force vs. separation profiles reveal film-thickness transitions as either single layers of ions, or ion pairs that are pushed with the sharp tip. The magnitude of the layering force—i.e. the force required to expel an IL layer—is a measure of the strength of the interaction between the ion and the substrate; a higher force indicates a stronger adsorption of the IL molecules either to the surface or to the underlying IL molecules. It is worthy of note that the magnitude of the layering force cannot be directly read from Figures 3-5, as the force isotherms were shifted for clarity. The layering force is shown in Figure 6a. The layered structure was most pronounced at the solid-IL interface, decaying with distance from the substrate surface and typically vanishing beyond ~3 layers.

A histogram of the number of layers found as a function of substrate roughness and counter-surface is shown in Figure SM3. With a sharp tip, most of the force measurements showed 2-3 interfacial layers on the 0 μm^{-2}-substrate, 1-2 on the 170 μm^{-2} substrate, and mostly 1, but often 2 layers on 1100 μm^{-2} substrates. Only 3% of the force isotherms showed 4 distinct layers. Hence, a more pronounced layering of the IL on a flat surface is demonstrated in these measurements.

The substrate roughness clearly played a significant role in determining the solid-like interfacial structure of the IL: the number of resolved layers during approach decreased with increased NP surface density.

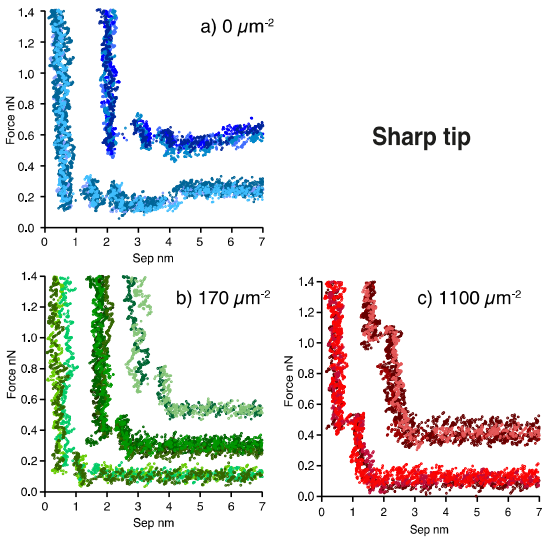

Figure 3: Representative force-distance curves (shifted in x and y for clarity) obtained with sharp tips (CSC38/No Al, radius <10 nm, 0.233 N/m, Mikromasch) on a silica substrate with NP surface densities of a) 0 μm^{-2}, b) 170 μm^{-2}, and c) 1100 μm^{-2}. Approach speeds of 30 nm s^{-1} and a maximum applied load of 8 nN were used. Force-separation curves were obtained in force maps over an area of 5μm x 5μm (576 force-distance curves).

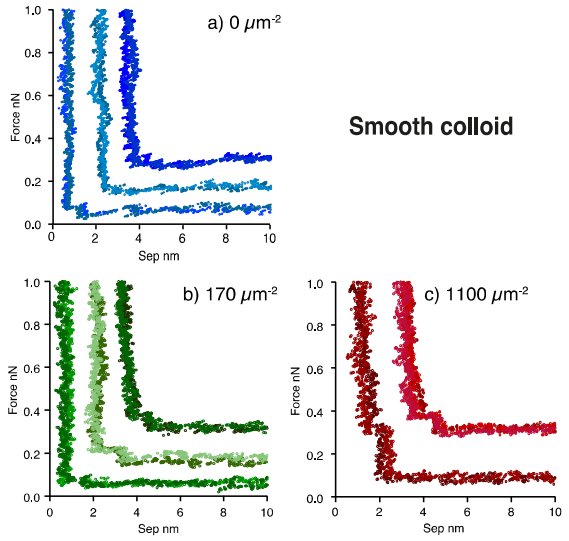

Figure 4: Representative force-distance curves (shifted in x and y for clarity) obtained with a smooth SiO_2 sphere colloid (RMS roughness ~2 nm) glued to a tipless cantilever (CSC37/tipless/Al Bs, 0.047 N/m, Mikromasch) on silica substrates with NP surface densities of a) 0 μm^{-2}, b) 170 μm^{-2} and c) 1100 μm^{-2}. Approach speeds of 30 nm s^{-1} and maximum applied loads of 8 nN were used. Force-distance curves were obtained in a force map over an area of 5 μm x 5 μm (576 force-distance curves).

Force measurements with a smooth colloid. Normal force vs. separation isotherms for [HMIM] Ntf2 nanoconfined between the substrate and the smooth colloid also reveal film-thickness transitions as either single layers of ions or ion pairs that are collectively squeezed out of the confined region (see Figure 4). Most of the force measurements showed 2-3 layers on the 0 μm^{-2} substrate, and the frequency of occurrence of 4 layers increased compared to the results with the sharp tip (figure SM3a), which is consistent with the expected enhancement of layering in nanoconfinement.[51] On both rough substrates, most of the force-distance curves showed 2 film thickness transitions, and 3 layers were less often detected than on the flat substrate, in agreement with a less ordered IL on rough substrates. Hence, similarly to the results with the sharp tip, the number of resolved layers decreased with increased NP surface density.

Force measurements with a rough colloid. Representative force isotherms between the silica substrates and a rough colloid are shown in Figure 5. Also in this case the force measurements reveal the presence of confined IL-layers. Figure SM3c shows that 2 layers were detected on flat and 170μm^{-2}-substrates, and a single layer on the 1100 μm^{-2}-substrates, demonstrating the lesser order of the IL in this non-conformal contact. It should be noted that the measured force isotherms with the rough colloid were noisier than with either smooth sphere or sharp tip.

Additional weakly adsorbed IL layers, i.e. with very low layering force, were measured with the smooth colloids, in agreement with reported values of up to 5 IL-layers elsewhere for other ILs and substrates. However, we have not analyzed them here due to the low frequency of occurrence of these layers (Figure SM3 b-c). Note that the steps in the force isotherm are superposed on the background noise, which is significant for the baseline and their clear discernment is difficult.

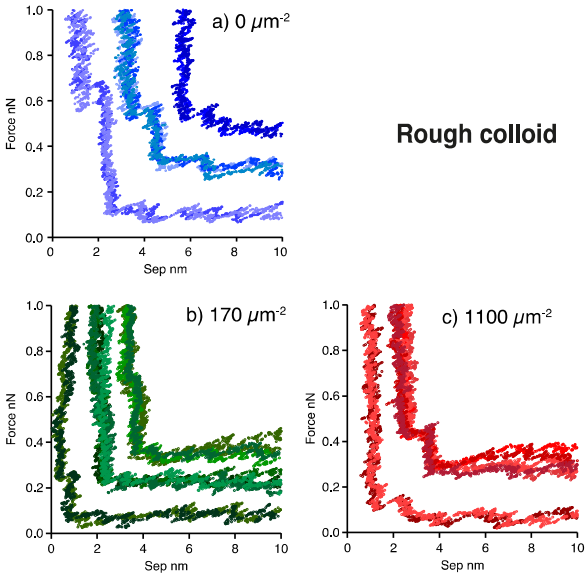

Figure 5: Representative force-distance curves (shifted in x and y for clarity) obtained with a rough SiO_2 colloid (RMS roughness =~9 nm) glued to a tipless cantilever (CSC37/tipless/Al Bs, 0.079 N/m, Mikromasch) on silica substrates with NP surface densities of a) 0 μm^{-2}, b) 170 μm^{-2}, and c) 1100 μm^{-2}. Approach speeds of 30 nm s^{-1} and a maximum applied load of 8 nN were used. Force-distance curves were obtained in force maps over an area of 5 μm x 5 μm (576 force-distance curves).

Characteristic Layering Forces

Figure 6 shows the layer size as a function of the layering force required to squeeze out an IL-layer. With the sharp tip (Figure 6a) on both rough substrates, layering is resolved at high layering forces F>~0.2 nN and at low layering forces F<0.02 nN with larger standard deviation (the layer thickness distributions are discussed in detail in the next section); these are not resolved on the flat substrate (see ellipses). The distribution of layering forces on the flat substrate is narrower (see arrow) than on the rough substrates. Compared to the behavior on the flat substrates, a larger layering force is required to squeeze out the layer closest to the hard wall on the rough substrates.

For the smooth sphere (Figure 6b), a similar behavior is observed at high layering forces (see ellipse), suggesting that the roughness of the substrate is responsible for this characteristically high layering force. At small layering forces, the distribution of layer thicknesses is much broader than that measured with a sharp tip on all substrates (see arrow): the layer size achieves values as high as 1.5 nm and there is no apparent correlation with the roughness of the substrate, indicating that confinement has modified the IL-interfacial structure.

In contrast, for the rough colloid (Figure 6c) there is no apparent correlation between layer size and NP surface density, suggesting that the counter-surface topography dominates the structure of the confined IL film. The distribution of layering forces is broad on all substrates. However, there is a trend to higher layering forces compared to the smooth colloid.

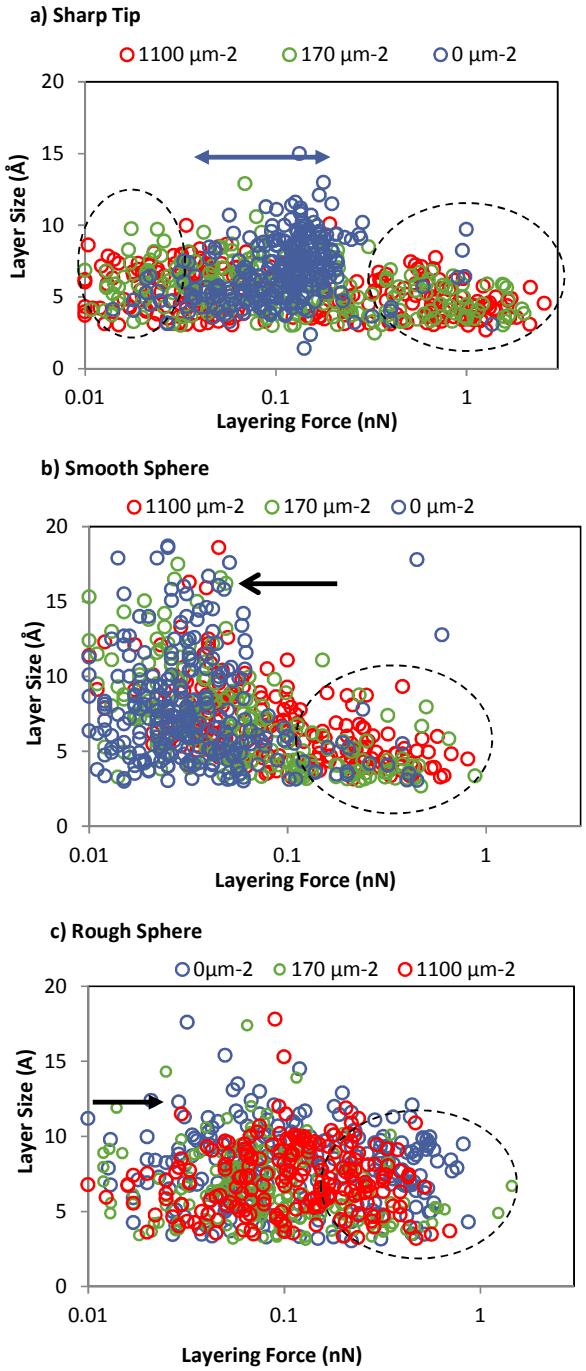

Figure 6: Layer size vs. layering force measured with **a)** sharp tip, **b)** smooth sphere and **c)** rough sphere on substrates with NP surface densities of 0 μm^{-2}, 170 μm^{-2}, and 1100 μm^{-2}. The ellipses and the arrows indicate the main differences between the substrates: a) highest and lowest layering forces are detected with the sharp tip on the rough substrates; b) largest layering force is measured with the smooth colloid on the rough substrates; the arrow points at the large magnitude of the measured layers at low layering forces on all substrates, which is likely caused by the confinement effect; c) similar layering forces on all substrates are detected with the rough colloid; the arrow indicates that the layering forces shift to higher values compared to those measured with the smooth colloid.

Characteristic Size of IL-Layers

The characteristic size of an IL-layer resolved in force measurements is not strictly equal to the true layer thickness, but to the change in the film thickness when a layer is squeezed out; we call this a film-thickness transition of characteristic size Δ ($\Delta=D_2-D_1$), where D_2 and D_1 are the film thickness at which the transition starts and ends, respectively (both with respect to the hard wall). To compare the characteristic size of the squeezed-out IL-layers for the different tip-substrate systems, we distinguish between the location of the layers (D_2) with respect to the hard wall (at an arbitrary zero): transition 1 is defined as the film thickness transition (or layer squeezed out from the contact) occurring closest to the hard wall ($D_1=0$), transition 2 is the next closest, and transition 3 is the furthest from the hard wall (see also arrows in Figure 3a). However, some ILnm-layers might not be detected in the force measurement, either because the layering force is small and superposed on the baseline, or because the applied force is not high enough. In fact, we cannot exclude that IL layers remain in the contact at the maximum applied force of 8 nN. Hence, transition 1 does not necessarily involve the squeezing out of the surface-adsorbed layer, since a boundary layer can remain adsorbed on the solid surface, as directly demonstrated in previous SFA studies[60].

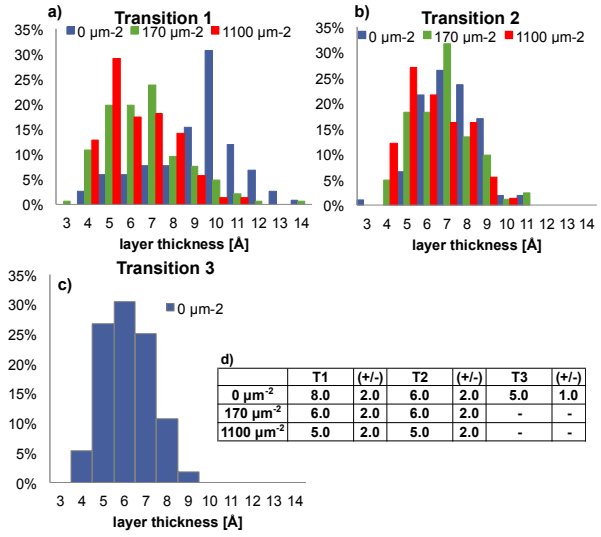

	T1	(+/-)	T2	(+/-)	T3	(+/-)
0 µm^{-2}	8.0	2.0	6.0	2.0	5.0	1.0
170 µm^{-2}	6.0	2.0	6.0	2.0	-	-
1100 µm^{-2}	5.0	2.0	5.0	2.0	-	-

Figure 7: Histograms for the measured characteristic size of IL-layers (interval =1 Å) with a sharp tip on 0, 170 and 1100 µm^{-2} substrates; b) Transition 1 is defined as the film-thickness transition occurring closest to the hard wall; b) transition 2 is the next closest, and c) transition 3 is the furthest from the hard wall. d) Characteristic thickness of each transition determined as the mean value of a binomial distribution fitted to the results. The second column gives the standard deviation.

Figure 7 shows the histograms for layer thicknesses (Δ) resolved with the sharp tip on the 3 substrates. Layer thicknesses smaller than 3 Å were very rare. We have used fits to a binomial distribution with a bin size of 1 Å to obtain the mean value, to compare results and highlight some differences. The characteristic size of transition 1 (Figure 7a) is much larger on the 0 µm^{-2}-substrate (Δ~8.1 Å) than on both the rough substrates, with the latter two showing similar characteristic sizes (Δ~5.6-5.2 Å). The distinct layer thickness for transition 1 is thus related to the presence of the NPs. Considering that the noise of the measured separation is ~1 Å, the difference between the measured thicknesses for transition 2 on all three substrates is not significant. For the flat substrate, the smaller size of transitions T2 and T3 compared to T1 indicates the different composition of the IL layers, in agreement with previous results in the literature[27,11]. The histogram in Figure 7c also demonstrates that IL layering on the two rough surfaces is clearly limited to two layers. Hence, NPs at both surface densities eliminate the occurrence of transition 3.

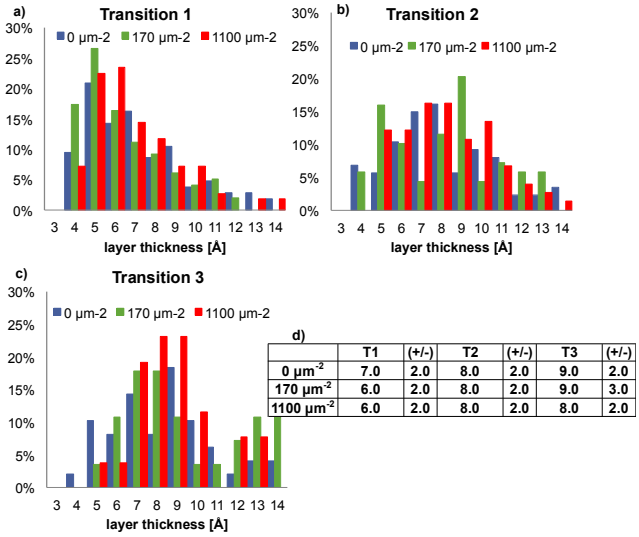

	T1	(+/-)	T2	(+/-)	T3	(+/-)
0 µm^{-2}	7.0	2.0	8.0	2.0	9.0	2.0
170 µm^{-2}	6.0	2.0	8.0	2.0	9.0	3.0
1100 µm^{-2}	6.0	2.0	8.0	2.0	8.0	2.0

Figure 8: Histograms for the measured layer thicknesses (interval =1 Å) with the smooth colloid (RMS roughness ~2 nm) on 0 µm^{-2}, 170 µm^{-2}, and 1100 µm^{-2} substrates. Transition 1 **a)** is defined as the film-thickness transition occurring closest to the hard wall, transition 2 **b)** is the next closest and transition 3 **c)** is the furthest from the hard wall. d) Characteristic thickness of each transition determined as the mean value of a unimodal binomial distribution fitted to the results. The second column gives the standard deviation.

Similar histograms were constructed for the measurements with the smooth silica colloid. Figures 8a-c show little difference between the layer-thickness distributions on the three substrates for the three significant film-thickness transitions. The distributions are broader than with the sharp tip and multiple peaks are visible. Since the fits using multiple distributions are poor and somehow arbitrary, the results in figure 8d are the result of a fit to a unimodal binomial distribution.

With the smooth colloid, the thickness of transition 1 is smaller than that of transitions 2 and 3, which differs from the results obtained with the sharp tip for the flat surface. It is to be noted that the structure of the nanoconfined IL film results from the overlap of the ion layers that form on both approaching surfaces, and that they will influence each other at separations smaller than ~2 nm. Hence, it is expected that the overlapped structure will differ from that formed on each single surface (and resolved with the sharp tip). Besides, in our case, due to the asymmetric nature of the confinement, the resulting nanoconfined film results from the superposition of two distinct layering patterns, which makes it difficult to

compare the layers resolved with the colloidal spheres. It is also interesting to note that transition 3 was resolved on both flat and rough substrates with the smooth sphere, in contrast to the results with the sharp tip (Figure 7c). This indicates that layering is enhanced with the size of the confined region, in agreement with results on molecular fluids[51]. The characteristic size of the layers is weakly sensitive to substrate roughness –it slightly decreases with increase in NP surface density, which is consistent with the idea that confinement plays a dominant role in the ordering of the IL.

Figure 9a-c show the histograms for the IL layer thicknesses resolved with the rough colloids; similarly to the smooth colloid, the distributions are broad. Figure 9d shows the mean and the standard deviation of the binomial distributions fitted to the results.

On the 170 μm^{-2} substrate, the characteristic size of transition 1 is smaller than that on the flat substrate; in fact it is similar to that resolved with the sharp tip and with the smooth colloid on the 170μm^{-2} substrate (5.6 Å). Moreover, no significant differences were observed for transition 2 measured with the two colloids on the 170 μm^{-2} substrate (7.3-7.8 Å). This suggests that the asperities on the colloids could behave as a sharp tip, thus leading to a single NP-colloid contact at low NP surface density. For the 1100 μm^{-2} substrate, the layer-thickness distribution differs from that obtained with the sharp tip and with the smooth colloid (see e.g. transition 1 in fig. 9a and 7a). As discussed later, multiple NP-colloid contacts are possible in this case.

Transition 3 is measured on 0 and 170 μm^{-2} substrates with the rough colloid, suggesting again that the larger contact geometry enhances ordering, as this transition was not observed with the sharp tip on the 170 μm^{-2} substrates (Figure 9c). In the rough contact between the 1100 μm^{-2} substrate and the rough colloid, a maximum of 2 layers was detected, i.e. less than with the smooth sphere, indicating that the IL adopts a more disordered structure when probed with the rough colloid.

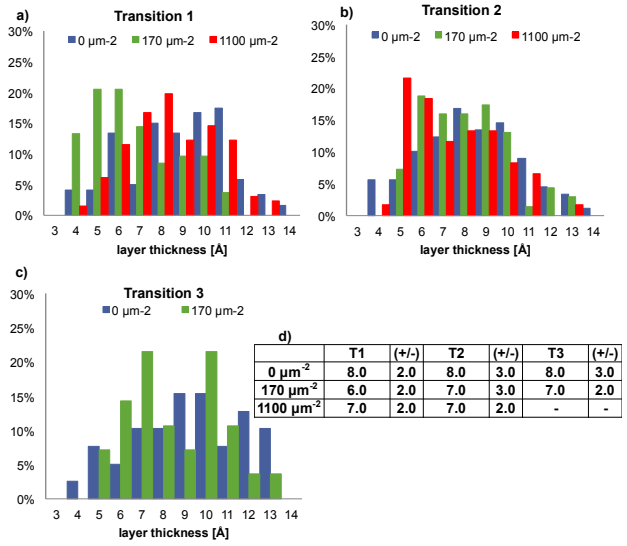

d)

	T1	(+/-)	T2	(+/-)	T3	(+/-)
0 μm^{-2}	8.0	2.0	8.0	3.0	8.0	3.0
170 μm^{-2}	6.0	2.0	7.0	3.0	7.0	2.0
1100 μm^{-2}	7.0	2.0	7.0	2.0	-	-

Figure 9: Histograms for the measured layer thicknesses (interval =1 Å) with the rough colloid (RMS roughness ~9 nm) on 0 μm^{-2}, 170 μm^{-2}, and 1100 μm^{-2} substrates. Transition 1 **a)** is defined as the film-thickness transition occurring closest to the hard wall, transition 2 **b)** is the next closest and transition 3 **c)** is the furthest from the hard wall. **d)** Characteristic thickness of each transition determined as the mean value of a binomial distribution fitted to the results. The second column gives the standard deviation.

We also note that transitions 2 and 3 resolved with a colloid (smooth and rough) are characteristically larger than those resolved with the sharp tip on the three substrates; this suggests that confinement significantly influences the structure of the nanoconfined IL and hence, the size of these transitions; a similar trend is not observed for transition 1, i.e. if IL-ions that are more strongly adsorbed to the surface are squeezed-out.

Discussion

The analysis of the measured force isotherms demonstrates the layered structure of [HMIM] Ntf2 on a variety of rough surfaces and rough contacts. In the force maps, each force isotherm is measured at a different location, with a distance of ~208 nm between these locations (24 isotherms are measured within 5 µm). Each force isotherm reveals the features of the out-of-plane-order of the IL within the area of contact, and the contact area varies as a function of substrate and tip. Heterogeneities within the 5µmx5µm area contribute to the broad distribution of layering forces and characteristic layer thicknesses. In-plane order may occur at the nanometer scale,[61, 62] but it is not resolved in force isotherms.

For comparison, Figure SM4a (Supplementary Information) shows selected force-distance isotherms—measured with a sharp tip on freshly-cleaved mica, i.e. an atomically flat surface. 50% of the force-distance curves obtained in force maps show a structural force with 2 distinct layers: $\Delta=6.6 \pm 2.3$ Å (transition 1) and $\Delta = 8.1 \pm 2.2$ Å (transition 2). The occurrence of a 3rd transition was rare. The layer characteristics differ from those obtained on a silica substrate, which indicates the different composition of the IL-interface. A strong interaction between the IL cation and mica is expected due to the negative charge of the surface that results from the dissolution of interfacial potassium ions—note that there are traces of water in the IL. This interaction is expected to be weaker on silica, which is consistent with an expansion of transition 1.

Layering behaviour of HMIM-Ntf2 in the rough contact

The asperities on the silica colloid probe affect short-range force interactions, i.e. the measured layering force and layer thickness (Figures 6-9). The following conclusions can be drawn from the measured distinctive layering:

(1) Despite the very small area occupied by NPs (1.9 % and 12 % of the total area of 170 μm^{-2} and 1100 μm^{-2} substrates, respectively), the transitions resolved with the sharp tip are strongly influenced by presence of the NPs (Figure 7). The decrease in characteristic size of transition 1 in the presence of the NPs (from 8.1 Å to ~5.2 Å) could mean that the tip resolves the layers on the NPs and they have a different size than on the flat portions of the substrate. However, this is very unlikely since the probability of hitting a NP is smaller than 12 % (in area). Another possible explanation for the different interfacial

structure is that it could be templated by the NPs on the substrate. This is an interesting result, as it suggests that nanopatterning could be used to control the solid-IL interfacial structure.

(2) Another notable difference is the characteristic thickness for transition 1 on the flat substrate: it is 8.1 Å when resolved with the sharp tip and ~6.6 Å with a smooth colloid (and with a very different distribution) (Figures 7a-8a). This change is accompanied by a slight decrease in the layering force (Figures 6a-b). SFA measurements of cyclohexane on mica contaminated with nanoparticles[63] showed smaller layering forces and smaller layer transitions for higher roughness-values, which was attributed to the higher disorder in the layers (defects). Similarly, previous AFM work also showed that larger tip radii led to smaller layering forces, which was proposed to result from the intrinsically larger roughness in larger tips, and local disorder at the asperities.[64] Although we see a reduction of the layering force for transition 1 with the tip/colloid roughness in agreement with these references, the layering force increases with the substrate roughness (see Figure 6a for the sharp tip and Figure 6b for the smooth colloid), which indicates that there is an additional mechanism of relevance in our measurements. To exclude the influence of cantilever twisting during the squeezing out of the IL, the lateral deflection was also recorded during the force measurement; the cantilever was observed to twist slightly only when pressing the hard wall, but the layers were squeezed out at lower pressures at which the lateral deflection was close to zero. Hence, we propose that the entrapment of the IL molecules in the non-conformal contact, and the hindered *flow through a tortuous path during the squeezing-out process* is responsible for our results. This will be justified in the following sections.

(3) Another significant result is that transition 3 is resolved on both rough substrates with the smooth colloid but not with the sharp tip. This is consistent with the *enhancement of the solid-like behaviour in confinement by the colloid,* which overcomes the more disordered interfacial IL-structure induced by the NPs. A similar conclusion can be derived from the results with the rough colloid for the 170 μm^{-2} substrate. It is likely that the roughness of the colloid smears out layering, which partially compensates the expected enhancement of layering in nanoconfinement, so that only one additional layer is clearly resolved. The broad distributions of layer thicknesses on rough substrates are consistent with adsorbed IL-layers with more defects, i.e. less solid-like, especially for the more weakly adsorbed layers (transitions 2 and 3).

(4) With the rough colloid (Figure 9), there are significant differences between the two rough substrates: transition 1 (closest to the hard wall) was significantly smaller on 170 μm^{-2} than on 1100 μm^{-2} substrates. Interestingly, the distribution on 170 μm^{-2} is reminiscent of that with the sharp tip, which points at similar contact geometries, while the distribution of transition 1 on 1100 μm^{-2} substrates is closer to that on flat substrates with the rough colloid. These results bring us to a discussion of the real contact geometry.

Entrapment of IL-molecules in the rough contact

Assume an ideal contact between a perfectly smooth sphere (R=5μm) and an atomically flat plane (both silica, E=72GPa, Poisson ratio=0.3). At the layering force of 1 nN, the sphere deforms under stress, and the (so-called) contact area or region has a diameter ∅ of ~9.2 nm according to the Hertz model.[65] The IL remains effectively confined in a slit pore constituted by two circular parallel plates of diameter 9.2 nm. Considering an average area per ion of ~0.38 nm^{-2} (with a cation diameter~0.7 nm), 170 ions *per layer* remain confined in this pore. For a sharp tip (with spherical curvature of R~10 nm) on an ideally smooth substrate, only ~3 ions/layer remain confined in the pore at an applied load of 1 nN. Hence, it is usually assumed that the tip does not induce confinement but it probes the interfacial structure of the IL on the flat substrate. Besides, one must also consider that a slower relaxation is possible if more molecules have to *collectively* leave the contact region, and this leads to a more pronounced solid-like behavior in the larger confining regions achieved with the colloid (and in SFA measurements) compared to the sharp tip.

Two approaches to modelling the rough contact were followed. An asymmetric rough contact can be modeled as a contact between flat and rough surfaces, the latter with an effective roughness that results from the (Weibull) distribution of the asperity heights of the two individual contacting rough surfaces.[66] The equivalent mean-square surface height Re^2 is given by the sum of that for each surface (from Figures 1c-2c), and it is assumed to characterize the rough contact. Figure 10a shows that the equivalent roughness of the asymmetric contact Re^2 gradually increases with the roughness of the substrate (2 to 16 nm^2 for the smooth colloid and 80 to 96 nm^2 for the rough colloid), whereas it abruptly increases if the rough colloid forms the contact instead of the smooth one. No roughness data is available for the sharp tip, but since its radius is three orders of magnitude smaller, a much smaller RMS roughness can be expected, and it will be assumed to be 0.4 nm as for the flat silica substrate. The difference in Re^2 of the contacts formed with the sharp tip and with the smooth sphere is shown to be small in Figure 10a. As the sharp tip-substrate contact is smaller than the distance between the NPs, the Weibull model could lead to misleading results for the contact Re^2; as comparison we have also calculated an area-averaged Re^2 for the sharp tip that considers the area coverage with NPs (see empty symbols in Figure 10a).

The second approach is based on the pull-off force to estimate the true contact area (Figure 10b).[56] The highest pull-off forces were obtained with the rough colloid, with the highest value for the flat surface (9.45 ± 0.70 nN), followed by the 1100μm^{-2} substrate (2.93 nN ± 0.24) and the 170 μm^{-2} substrate (1.16 nN±0.12), suggesting the order of decreasing contact area of these non-conformal contacts. A similar trend was obtained for the smooth colloid but smaller pull-off forces were observed (2.74 ±0.20 nN on the flat substrate; 1.57 ±0.15 nN on the 1100 μm^{-2} and 1.2±0.11 nN on the the 170 μm^{-2} substrate). Again, this indicates the same order in true contact

area, but with a smaller value than for the rough sphere. In contrast, for the sharp tip a slightly higher pull-off force was obtained for the 1100 µm^{-2} (1.78 ±0.18 nN) whereas the pull-off force for the 0 and 170 µm^{-2} substrates was statistically similar (1.55±0.17 nN and 1.42±0.18 nN, respectively) and slightly smaller than for the 1100 µm^{-2} substrate, suggesting that the true contact area is very similar for the 3 substrates. It is worthy of note that the sharp tip is made of silicon, which is expected to be covered by a thin passivation layer of oxide, but the surface-interaction forces might differ from those of the silica colloid due to a different OH-surface density, which could explain the different adhesion.

Various theories can be applied to relate the pull-off force L to the true contact area A_0. One of these theories is the Johnson-Kendall-Roberts (JKR) model. The JKR model assumes a flat contact, which is not the case in the presence of asperities and therefore it provides only a rough estimation for our systems but it is sufficient for our purpose. According to the JKR model, the contact area A_0 is proportional to $L^{2/3}$. This relation helps to interpret the contact geometry.

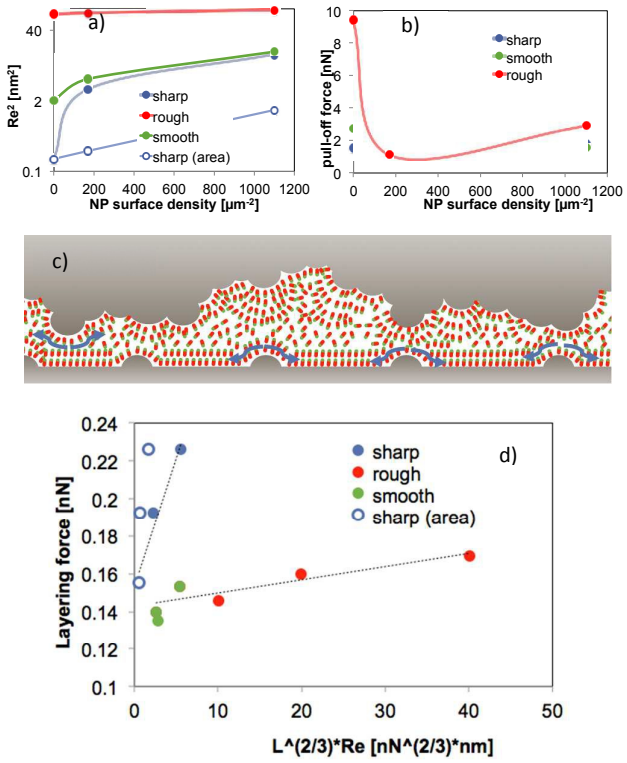

Figure 10: a) Equivalent roughness Re^2 b) and pull-off force as a function of the NP-surface density for the three tips. Error bars are smaller than the symbol size. C) Schematics of the contact between rough sphere and 1100 µm^{-2} substrate; d) Correlation between the layering force F (F>0.05 nN) and the $L^{\wedge}(2/3) * Re$-parameter.

We note that the pull-off force on the 170 µm^{-2} substrate is similar for smooth and rough colloids, thus indicating the same true contact area for all of them with this substrate (see minimum in Figure 10b). Simple geometrical considerations show that the true contact is given by one, or at most two NP-colloid contacts considering the large distance between the NPs and the roughness features. The roughness of the NPs is unknown, but multiple asperities at the nanoscale cannot be ruled out and will also affect the true contact. Based on the increase in pull-off force observed for the 1100µm^{-2} substrate, we conclude that more than 2 NPs can be in contact with the rough sphere in this case (Figure 10c). Note that although the ideal flat contact has a diameter of ~9 nm, the large asperity-to-valley distances and the irregular shapes of these asperities can lead to contact with several NPs and even with the flat portion of the substrate. The large pull-off force for the 0 µm^{-2} substrate suggests that more multi-asperity contacts are possible on the flat substrate compared to the 170 µm^{-2} substrate, i.e. the NPs reduce the contact area. According to the roughness characteristics of the smooth colloid and the pull-off force we expect only contact with one or two NPs on both rough substrates.

Figure 10c shows a very simple representation of the rough confinement. Upon approach of the colloid, IL-layers are squeezed out at different forces and separations (leading to the broad layer-thickness distributions); however at each asperity, the layered structure is still preserved. Thus, despite the difficulties in resolving the layers in a rough contact, our results demonstrate the layered structure of [HMIM] Ntf2 between confined rough interfaces.

When the two surfaces approach each other, the IL is squeezed out and a load is applied to remove the strongly adsorbed layers. The arrows in Figure 10c indicate the "flow" of the squeezed IL-layers. The contact consists of a tortuous nanoporous network, and the IL molecules flow in between the asperities, possibly with an enhanced viscosity, as suggested for confined ILs in a previous work.[14] The higher tortuosity of the porous network leads to smaller permeability, and thus, higher forces need to be applied. We note that the tortuosity represents the tortuous path of the IL molecules as they are squeezed out, and therefore it is related to the effective roughness of the contact, thus to $(Re^2)^{0.5}$.

To model IL-squeezing, we assume that (i) the squeezing out of ions follows Darcy's law ($\Delta m/A\Delta t \propto k\Delta p/r$), where the permeability decreases with increase in tortuosity of the porous network,[67] (ii) the force to squeeze the IL-molecules depends on the contact geometry ($F \sim \Delta p A_0$), and (iii) the mass rate remains approximately constant. The contact radius r presents the size of the confinement region. The tortuosity of the porous network is assumed to be directly proportional to *Re*. The IL viscosity could be enhanced in confinement but we assume it to be the same for the ILs in all contacts. Under these very simple conditions, the following relation is obtained for the layering force: $F \sim \alpha A_0 * Re$, where α is not unitless. According to the JKR model, $F \sim L^{2/3} * Re$. Figure 10d shows the correlation between the layering force and $L^{2/3} * Re$. A satisfactory trend is obtained for the colloids, which supports the idea that an entrapment of IL-molecules occurs during the squeezing-out process between rough surfaces. On the other hand, the much larger layering force measured with the sharp tip could be caused by the more pronounced order of the IL in this case, and by the different interfacial composition on flat and rough substrates, as discussed previously, and partially compensated by the smaller contact radius, r. Similar trends

are obtained for both calculated Re-values. Further studies are needed to clarify this difference.

Conclusions about the composition of the IL-layers are difficult, because of the broad distribution of IL-layer thicknesses. This has been attributed to weak interactions between ILs and silica. Considering silica is slightly negatively charged, a cation-enriched layer is expected[32, 68], which has a size of 8.1 Å on the flat substrate and 5.6-5.2 Å on the rough substrates, as resolved with the tip. These layer thicknesses suggest that the NPs could template a more tilted orientation of the hexyl chain on the rough substrates. It is, however, also possible that the 8.1 Å layer is composed of ion pairs and the 5.6-5.2 Å layer is composed mostly of anions due to a strongly bound cation layer that cannot be removed. The latter scenario seems less likely, since a similar interaction strength between the cation layer and rough and flat surfaces is expected, and a high force (in some experiments up to 40 nN) was applied. Nevertheless, both scenarios indicate a change in layer size and composition due to the presence of nanoparticles.

Finally, a few words are needed about the formation kinetics of the interfacial structure. The *equilibrium* interfacial IL-layers are perturbed during each single force measurement, as the molecules are squeezed out from the contact. In force maps, different positions on the substrate are consecutively probed, and therefore it can be assumed that the unperturbed interfacial IL-structure on the substrate is always resolved. However, the question is whether the interfacial IL-structure on the colloid can be recovered between consecutive approaches, specifically, within ~11 s under the conditions of the force maps. The self-diffusion coefficient of [HMIM] Ntf2 has been reported to be 4 x 10^{-7} cm^2/s,[69] thus, it takes ~ 0.64 ms for the ions to diffuse a distance of 160 nm, which is the force separation. Although IL diffusion is sufficiently fast, the adsorption/desorption of IL onto silica could take longer. To investigate whether silica-related interfacial processes could retard the formation of the equilibrium interfacial IL-layers, continuous force measurements were performed at a single location with a smooth colloid on a flat silica substrate. The time delay between consecutive force measurements was varied between 11 s and 7 min. Ten force isotherms with resolved layers were obtained for each time delay. While shorter delays between force measurements yielded a higher percentage of curves lacking resolved layers (~15% and 20% for 2 min and 11 s, respectively) caused by the perturbed interfacial structure on both counter-surfaces, the layering force, layer thicknesses and the number of resolved layers per force isotherm were statistically similar for all investigated conditions (see Figure SM5). Thus, we conclude that the IL-layer structure resolved in force maps corresponds to an equilibrium structure on silica surfaces, and it provides better statistics for heterogeneous substrates.

The existence of a structural force for [HMIM] Ntf2 in a rough contact is of interest because the current understanding is that a randomly rough surface of only a few angstroms is sufficient to eliminate oscillatory forces. These results suggest that the interfacial (layered) structure is perturbed but the IL molecules at rough interfaces can behave cooperatively over localized regions, i.e., around the asperities. The variation in force-curve measurements arises from the specific non-conformal contact, which could change during experiments, for example, if the asperities were to plastically deform or break at higher forces. This can be excluded in the reported results as the pull-off force, as well as the layering statistics, were observed to remain constant within the force map. From this study, we conclude that the interfacial IL structure does not entirely vanish in a rough contact with characteristic roughness features larger than the molecular size of the IL. According to these results, nanoscale roughness could be a way to modify or tune the interfacial properties of ILs.

Conclusions

Force-separation isotherms were reported for [HMIM] Ntf2 on various smooth and rough surfaces measured with a sharp tip. The arrangement of the interfacial layers is modified by the presence of NPs at the surface. Since the surface coverage of NPs is low, the results could imply that the NPs also induce a change of the interfacial IL structure within the flat regions of the substrate. An alternative explanation is that the NPs could block the displacement of the IL-layers and this would lead to a perturbed displacement of layers with a distinct “effective” layer size.

Interfacial IL-layering was also measured with smooth and rough colloids. The induced confinement enhanced the solid-like behaviour of [HMIM] Ntf2—i.e. the number of resolved layers—but the confinement effect was partially counterbalanced by the increase in the number of NP-colloid contacts. Transitions at low layering force were not clearly detected, which we attribute to more defective—less well-ordered—layers, but also to the higher noise of the force-isotherm baseline measured with colloids. We propose that the resolved layers in the structural force result from local ordering at the multi-asperity contacts. An entrapment of the IL molecules at the rough contact can explain the observed changes in the structural forces.

The results of this study demonstrate that layering may occur at the contact between sliding rough surfaces and in electrode carbon nanopores, but that extrapolation of layering forces and layer thicknesses, i.e. the composition and arrangement of IL molecules, obtained on flat surfaces to real systems may not be possible. As a consequence, laboratory studies that better represent the real rough contact are needed to understand the performance of ILs in applications more completely. The dynamics of the IL molecules at rough contacts remain an open question.

Acknowledgements

We thank the Environmental Engineering Fellowship Program for funding Alexis Sheehan’s research, and the Swiss National Science

Foundation for financial support. Colloidal-probe atomic force microscopy measurements were carried out in the Frederick Seitz Materials Research Laboratory Central Research Facilities, University of Illinois.

Notes and references

1. C. Ye, W. Liu, Y. Chen and L. Yu, *Chem Commun*, 2001, DOI: 10.1039/B106935G, 2244-2245.
2. M. Palacio and B. Bhushan, *Tribol Lett*, 2010, **40**, 247-268.
3. M.-D. Bermúdez, A.-E. Jiménez, J. Sanes and F.-J. Carrión, *Molecules*, 2009, **14**, 2888-2908.
4. M. Armand, F. Endres, D. R. MacFarlane, H. Ohno and B. Scrosati, *Nat Mater*, 2009, **8**, 621-629.
5. D. R. MacFarlane, N. Tachikawa, M. Forsyth, J. M. Pringle, P. C. Howlett, G. D. Elliott, J. H. Davis, M. Watanabe, P. Simon and C. A. Angell, *Energ Environ Sci*, 2014, **7**, 232-250.
6. S. J. Zhang, N. Sun, X. Z. He, X. M. Lu and X. P. Zhang, *J Phys Chem Ref Data*, 2006, **35**, 1475-1517.
7. W. R. Jones, B. A. Shogrin and M. J. Jansen, *Journal of Synthetic lubrication*, 2000, **17**, 109-122.
8. R. G. Horn, D. F. Evans and B. W. Ninham, *J Phys Chem-Us*, 1988, **92**, 3531-3537.
9. O. Werzer and R. Atkin, *Physical Chemistry Chemical Physics*, 2011, **13**, 13479-13485.
10. H. Li, M. W. Rutland and R. Atkin, *Phys Chem Chem Phys*, 2013, **15**, 14616-14623.
11. A. M. Smith, K. R. J. Lovelock, N. N. Gosvami, P. Licence, A. Dolan, T. Welton and S. Perkin, *J Phys Chem Lett*, 2013, **4**, 378-382.
12. S. Perkin, *Physical Chemistry Chemical Physics*, 2012, **14**, 5052-5062.
13. S. Perkin, L. Crowhurst, H. Niedermeyer, T. Welton, A. M. Smith and N. N. Gosvami, *Chemical Communications*, 2011, **47**, 6572-6574.
14. S. Perkin, T. Albrecht and J. Klein, *Physical Chemistry Chemical Physics*, 2010, **12**, 1243-1247.
15. T. Carstens, R. Hayes, S. Z. El Abedin, B. Corr, G. B. Webber, N. Borisenko, R. Atkin and F. Endres, *Electrochimica Acta*, 2012, **82**, 48-59.
16. M. Mezger, H. Schroder, H. Reichert, S. Schramm, J. S. Okasinski, S. Schoder, V. Honkimaki, M. Deutsch, B. M. Ocko, J. Ralston, M. Rohwerder, M. Stratmann and H. Dosch, *Science*, 2008, **322**, 424-428.
17. R. Capozza, A. Vanossi, A. Benassi and E. Tosatti, *arXiv preprint arXiv:1412.7445*, 2014.
18. A. M. Smith, K. R. Lovelock, N. N. Gosvami, T. Welton and S. Perkin, *Phys Chem Chem Phys*, 2013, **15**, 15317-15320.
19. J. Hoth, F. Hausen, M. H. Müser and R. Bennewitz, *Journal of Physics: Condensed Matter*, 2014, **26**, 284110.
20. Y. Lauw, M. D. Horne, T. Rodopoulos, V. Lockett, B. Akgun, W. A. Hamilton and A. R. J. Nelson, *Langmuir*, 2012, **28**, 7374-7381.
21. B. Fitchett and J. Conboy, *The journal of physical chemistry. B*, 2004, **108**, 20255-20262.
22. T. Cremer, M. Cremer, A. Stark, H. P. Deyko and Maier, *Langmuir*, 2011, **27**, 3662-3671.
23. B. Uhl, T. Cremer, M. Roos, F. Maier, H. P. Steinruck and J. Behm, *Physical Chemistry Chemical Physics*, 2013, **15**, 17295-17302.
24. T. Cremer, C. Kolbeck, K. R. J. Lovelock, N. Paape, R. Wolfel, P. S. Schulz, P. Wasserscheid, H. Weber, J. Thar, B. Kirchner, F. Maier and H. P. Steinruck, *Chem-Eur J*, 2010, **16**, 9018-9033.
25. A. Deyko, T. Cremer, F. Rietzler, S. Perkin, L. Crowhurst, T. Welton, H. P. Steinruck and F. Maier, *J Phys Chem C*, 2013, **117**, 5101-5111.
26. A. Arcifa, A. Rossi, R. M. Espinosa-Marzal and N. D. Spencer, *The Journal of Physical Chemistry C*, 2014, **118**, 29389-29400.
27. H. Li, F. Endres and R. Atkin, *Physical Chemistry Chemical Physics*, 2013, **15**, 14624-14633.
28. X. Zhang, Y. X. Zhong, J. W. Yan, Y. Z. Su, M. Zhang and B. W. Mao, *Chem Commun*, 2012, **48**, 582-584.
29. R. Köhler, J. Restolho, R. Krastev, K. Shimizu, J. N. Canongia Lopes and B. Saramago, *The Journal of Physical Chemistry Letters*, 2011, **2**, 1551-1555.
30. Y. Yokota, T. Harada and K.-i. Fukui, *Chem Commun*, 2010, **46**, 8627-8629.
31. S. Bovio, A. Podestà, C. Lenardi and P. Milani, *The Journal of Physical Chemistry B*, 2009, **113**, 6600-6603.
32. R. Atkin and G. G. Warr, *The Journal of Physical Chemistry C*, 2007, **111**, 5162-5168.
33. Y. Liu, Y. Zhang, G. Wu and J. Hu, *J Am Chem Soc*, 2006, **128**, 7456-7457.
34. R. M. Espinosa-Marzal, A. Arcifa, A. Rossi and N. D. Spencer, *The Journal of Physical Chemistry Letters*, 2014, **5**, 179–184.
35. R. M. Espinosa-Marzal, A. Arcifa, A. Rossi and N. D. Spencer, *J Phys Chem C*, 2014, **118**, 6491–6503.
36. M. A. Gebbie, M. Valtiner, X. Banquy, E. T. Fox, W. A. Henderson and J. N. Israelachvili, *P Natl Acad Sci USA*, 2013, **110**, 9674-9679.
37. A. M. Smith, K. R. J. Lovelock, N. N. Gosvami, T. Welton and S. Perkin, *Phys Chem Chem Phys*, 2013, **15**, 15317-15320.
38. M. A. Gebbie, M. Valtiner, X. Banquy, W. A. Henderson and J. N. Israelachvili, *Proceedings of the National Academy of Sciences*, 2013, **110**, E4122.
39. A. A. Lee, D. Vella, S. Perkin and A. Goriely, *The Journal of Physical Chemistry Letters*, 2014, DOI: 10.1021/jz502250z.
40. S. Perkin, M. Salanne, P. Madden and R. Lynden-Bell, *Proceedings of the National Academy of Sciences*, 2013, **110**, E4121.
41. A. J. Page, A. Elbourne, R. Stefanovic, M. A. Addicoat, G. G. Warr, K. Voitchovsky and R. Atkin, *Nanoscale*, 2014, **6**, 8100-8106.
42. I. Bou-Malham and L. Bureau, *Soft Matter*, 2010, **6**, 4062-4065.
43. O. Y. Fajardo, F. Bresme, A. A. Kornyshev and M. Urbakh, *Sci. Rep.*, 2015, **5**.

44. H. Li, R. J. Wood, M. W. Rutland and R. Atkin, *Chem Commun*, 2014, **50**, 4368-4370.
45. H. Li, F. Endres and R. Atkin, *Phys Chem Chem Phys*, 2013, **15**, 14624-14633.
46. K. Ueno, M. Kasuya, M. Watanabe, M. Mizukami and K. Kurihara, *Phys. Chem. Chem. Phys.*, 2010, **12**, 4066-4071.
47. R. Espinosa-Marzal, A. Arcifa, A. Rossi and N. Spencer, *The Journal of Physical Chemistry Letters*, 2013, **5**, 179-184.
48. R. M. Espinosa-Marzal, A. Arcifa, A. Rossi and N. D. Spencer, *The Journal of Physical Chemistry C*, 2014, **118**, 6491-6503.
49. H.-W. Cheng, P. Stock, B. Moeremans, T. Baimpos, X. Banquy, F. U. Renner and M. Valtiner, *Advanced Materials Interfaces*, 2015, **2**, n/a-n/a.
50. K. Sakai, K. Okada, A. Uka, T. Misono, T. Endo, S. Sasaki, M. Abe and H. Sakai, *Langmuir*, 2015, **31**, 6085-6091.
51. J. N. Israelachvili, *Intermolecular and Surface Forces: Revised Third Edition*, Elsevier Science, 2011.
52. K. Yang, Y. Lin, X. Lu and A. V. Neimark, *Journal of Colloid and Interface Science*, 2011, **362**, 382-388.
53. J. M. Black, M. Baris Okatan, G. Feng, P. T. Cummings, S. V. Kalinin and N. Balke, *Nano Energy*, 2015, **15**, 737-745.
54. G. Feng, S. Li, W. Zhao and P. T. Cummings, *AIChE Journal*, 2015, **61**, 3022-3028.
55. S. Ramakrishna, R. M. Espinosa-Marzal, V. Naik, P. C. Nalam and N. D. Spencer, *Langmuir*, 2013, **29**, 15251–15259.
56. S. N. Ramakrishna, L. Y. Clasohm, A. Rao and N. D. Spencer, *Langmuir*, 2011, **27**, 9972-9978.
57. C. Huwiler, T. P. Kunzler, M. Textor, J. Voros and N. D. Spencer, *Langmuir*, 2007, **23**, 5929-5935.
58. B. E. Deal and A. S. Grove, *J Appl Phys*, 1965, **36**, 3770-&.
59. J. L. Hutter and J. Bechhoefer, *Rev Sci Instrum*, 1993, **64**, 1868-1873.
60. R. M. Espinosa-Marzal, A. Arcifa, A. Rossi and N. D. Spencer, *The Journal of Physical Chemistry C*, 2014, **118**, 6491–6503.
61. A. Elbourne, S. McDonald, K. Voïchovsky, F. Endres, G. G. Warr and R. Atkin, *Acs Nano*, 2015, **9**, 7608-7620.
62. Z. Yan, D. Meng, X. Wu, X. Zhang, W. Liu and K. He, *The Journal of Physical Chemistry C*, 2015, **119**, 19244-19252.
63. M. Heuberger and M. Zach, *Langmuir*, 2003, **19**, 1943-1947.
64. S. J. O'Shea, N. N. Gosvami, L. T. W. Lim and W. Hofbauer, *Jpn J Appl Phys*, 2010, **49**.
65. H. Hertz, *J. Reine Angew. Math*, 1881, **92**, 156.
66. N. Yu and A. A. Polycarpou, *Journal of tribology*, 2004, **126**, 225-232.
67. P. C. Carman, *The Journal of Agricultural Science*, 1939, **29**, 262-273.
68. M. Mezger, H. Schröder, H. Reichert, S. Schramm, J. S. Okasinski, S. Schöder, V. Honkimäki, M. Deutsch, B. M. Ocko, J. Ralston, M. Rohwerder, M. Stratmann and H. Dosch, *Science*, 2008, **322**, 424-428.
69. H. Tokuda, K. Hayamizu, K. Ishii, M. A. B. H. Susan and M. Watanabe, *The Journal of Physical Chemistry B*, 2005, **109**, 6103-6110.